Use of the digital image correlation and acoustic emission technique to study the effect of structural size on cracking of reinforced concrete

Syed Yasir Alam, Ahmed Loukili, Frédéric Grondin, Emmanuel Rozière

Use of the digital image correlation and acoustic emission technique to study the effect of structural size on cracking of reinforced concrete

S.Y. Alam *, A. Loukili, F. Grondin, E. Rozière

LUNAM Université, Ecole Centrale de Nantes, Institut de Recherche en Génie Civil et Mécanique (GeM), UMR-CNRS 6183, 1 rue de la Noë, 44321 Nantes, France

An experimental investigation is performed to study the degradation of reinforced concrete beams by employing two experimental techniques simultaneously i.e. digital image corre lation and acoustic emission. The former method gives very precise measurement of sur face displacements, thus crack openings and crack spacing are determined. In order to complement this method and to investigate damage mechanisms, acoustic emissions resulting from internal damage are also analysed. Beams of three different sizes but pro portionally similar, are tested to study the effect of structural size. A comparison of the experimental measurements with Eurocode expressions is also presented.

1. Introduction

Cracking of concrete due to its weaker tensile strength is one of the common causes of damage in concrete structures and results in huge annual cost to the construction industry. Crack openings in large amounts cause corrosion of the reinforce ment and deterioration of concrete which affect the durability of the structure and can also lead to loss of load bearing capac ity in case of excessive damage. Corrosion damage can be in the form of reduction in cross sectional area of the reinforcing bars or in loss of bar anchorage due to surface spalling. Loss of anchorage means that reinforcing bars are not able to develop their useable strength. Increased permeability can also occur because of excessive crack openings that affects the overall integrity of the concrete [33], such as sulphate attack [39,16] or alkali aggregate reactivity.

In order to predict fracture of concrete, material size effect has fundamental importance. Nominal strength always decreases with the increase in the size of specimen. The mechanical behaviour of concrete becomes quasi brittle at labora tory scale with more strength controlled failure for notched specimens; however, at sufficient large scale the behaviour tends to become perfectly brittle [4]. The question of material size effect has become a crucial consideration in the efforts to design concrete structures, for which there inevitably is a large gap between the scales of large structures (dams, reactor contain ments, bridges) and of laboratory tests. Among the different theories of material size effect, Bazant [4] established that a deterministic size effect on nominal strength is caused by the presence of large Fracture Process Zone (FPZ) of a characteristic size which always precedes discrete macrocracks. A large amount of energy is consumed by various toughening mechanisms

* Corresponding author. Tel.: +33 (0) 2 40 37 16 61.
E-mail address: syed-yasir.alam@ec-nantes.fr (S.Y. Alam).

Nomenclature

f_{yk}	yield strength of steel bars
b	thickness of beam
h	height of beam
L	length of beam
l	support span
ρ	reinforcement ratio
w_k	design crack width
$s_{r,max}$	maximum crack spacing
ε_{sm}	mean strain in the reinforcement
ε_{cm}	mean strain in concrete between cracks
σ_s	stress in the tension reinforcement
A_s	area of tension reinforcement
$A_{c,eff}$	effective tension area of concrete around the steel
ϕ	steel bar diameter
k_1, k_2	coefficients depending upon steel concrete bond properties
c	concrete cover thickness

occurring in the FPZ, such as microcracking and aggregate interlock [43]. Various studies have been performed to understand the cracking mechanism in concrete; it is observed that cracking process is influenced by the structure size [3,14]. In plain concrete specimens of proportional sizes and using an experimental method based on Digital Image Correlation (DIC) tech nique, [1,2] have investigated material size effect on fracture propagation. The studies indicated a significant effect of the specimen size on the cracking mechanism in plain concrete.

In reinforced concrete beams, effect of structural size has been investigated on overall strength in numerous studies [24,6,45]. The results confirm that the bearing capacity of beam decreases with increasing beam size. True material size effect on concrete failure process in reinforced concrete beams is a complicated issue. True material size effect on concrete failure process in reinforced concrete beams is a complicated issue. Due to presence of reinforcement bars, multiple cracks propagate at the same time and the boundaries of FPZ for each crack overlap. Also there are other important factors that influence the failure modes such as shear span to beam effective depth ratio (a/d) [24], reinforcement ratio (ρ) [48,11] and beam depth (h) [6]. Beam fails in shear when the depth is low and shear to effective depth ratio is high. While studying the effect of structural size over a size range of 1:16 (h = 25 406 mm, a/d = 3 and ρ = 1.65%) in geometrically similar beams, [6] Bazant and Kazemi found that smaller beams fails in flexure, while larger beams fails in shear. [47] Syroka Korol and Tejchman found that in bending beams (a/d = 3 and ρ = 1%) failure process is usually preceded by tensile cracks as soon as concrete tensile strength is reached. The population of tensile cracks increases during the strain hardening phase. The bond between concrete and steel activates during this phase. In case of deformed bars, wedging action effectively increases the bond strength and internal microcracking takes place near the steel bar [28].

Although studies have shown the effect of structural size on bearing capacity of reinforced concrete beams, not much work has been done to investigate the effect on fracture parameters (such as crack openings and crack spacing). A numerical study [32] based on fracture mechanics model has shown the cracking behaviour to be size dependant. They found that crack width decreases as the width of the member increases. It was noted that previously obtained experimental data is very scat tered because crack width depends not only on the geometry and loading condition of the structure, but also on the size of structure. It should also be noted that in reinforced concrete beams, failure can be due to tensile cracking, steel concrete bond failure, shear cracking, or compression failure. Material size effect on these individual failure processes have been investigated by many researchers e.g. tensile cracks [4,31] in shear [5,6], steel concrete bond [40,20]; compression failure [9,50]. However, an interesting point is that in most circumstances, the failure process is the combination of above processes. In this paper our focus is to investigate the effect of structural size in reinforced concrete bending beams (where combined failure modes are expected to occur). When the loadings are lower (under serviceability limits), steel concrete bond is intact and the crack openings and crack spacing are linked with the strain in steel. However; when loadings increase (beyond ser viceability limits) crack opening are not only due to strain in steel but also due to the bond failure at steel concrete interface and macrocrack propagation. For such loadings, where combined failure modes are occurring it is important to study the effect of structural size on crack opening and crack spacing which strongly affect the durability of concrete. Such transition of failure modes are usually not taken into account in design codes and will be examined further in this paper.

The objectives of this paper are to present experimental results and to analyse the effect of structural size on the cracking process. Three sizes of beams with geometrically similar length and height, but with constant thickness are tested in three point bending. The tensile reinforcement ratio is kept constant; however, the concrete cover to the reinforcement

was scaled according to the overall size of the beam. The DIC technique is used to determine the discrete macro crack features such as crack opening and crack spacing. However, the acoustic emission (AE) technique is employed to follow the microcracking in the reinforced concrete beams. Also, a comparison for the concrete crack width and crack spacing is presented between Eurocode expressions [17] and experimental measurements.

2. Experimental program

2.1. Materials

The concrete used to prepare the beams was made from Portland cement type 52.5, sand, aggregate and water using the mix proportions in Table 1. The compressive strength of concrete was tested at 28 days using ϕ 11 $\times$ 22 cm^2 cylindrical specimens and was found to be 40 MPa. Since the beams were reinforced with rebars, a super plasticizer with a dosage of 0.25% by weight of cement was added to increase the workability of fresh concrete.

The longitudinal reinforcement of beams was constituted of deformed bars with 10, 14 and 20 mm in diameter, while, the transverse reinforcement was provided by deformed bars with 6 mm in diameter. The steel bars in both cases were type $f_{yk} \geqslant 500$ MPa.

2.2. Specimen details

Three point bending tests were conducted on three sizes of beams. The dimensions of beams are given in Table 2. The sizes of beams conform to [36] recommendations of size effect test. The beams are hereafter designated as D1, D2 and D3 for smaller, medium and large sized beam. The beams had a constant width (b = 100 mm), however, the total length (L), the support span (l) and height (h) were scaled. Concrete cover at the tension face of the beam was also scaled with same proportion between different sizes of beams. The beams were reinforced with a constant reinforcement ratio (ρ) by varying the diameter of bars; however, the number of bars was kept constant. During our experiments, near mid span, shear forces are very small and flexural forces are dominant. However, on the outer part of the beam (away from mid span), shear forces increase. Transversal reinforcement was thus provided only on the outer sides of beam and designed using typical design equations of Eurocode 2 [17]. Two hanger bars of 6 mm diameter were used to support steel stirrups. These bars were cut where the stirrups were not provided (Fig. 1).

2.3. Test procedure

All experiments were performed using the servo hydraulic universal testing machine with controlled displacement. The test setup is shown in Fig. 2. The load was applied at mid span with a cylindrical jack, ensuring the point load. The load was transferred to the beam using a rubber pad to avoid concrete damage at the load point. All the tests were carried out using a constant vertical displacement rate of 0.5 mm/min. Because the depth of the specimen varies, the loading rate in terms of structural behaviour (such as strain in the reinforcement would be different for each specimen i.e. lower effective loading rate (in terms of strain) for the larger specimens. In this study, the effect of different effective loading rate on the failure process is assumed not significant and therefore has not been studied in work. For each beam, electric strain gauges were attached on the lower face of each tension steel bar at mid span to measure the longitudinal strain in steel during the test (Fig. 3). After casting, the beams were stored at 20 °C ± 2 °C and covered with a plastic sheet to avoid the drying. After the removal of moulds, beams were stored in 100% relative humidity for 28 days in lime water to prevent the lixiviation and the drying shrinkage. The tests were performed in three point loadings to provide similar loading setup for all three sizes of beams in order to investigate effect of structural size. The beams were rested on steel rollers as the supports and load was applied by a steel loading jack.

2.4. Digital Image Correlation (DIC) setup

During the experiments, one side of the beam was subjected to displacement measurement using DIC technique. It is an effective optical method to measure surface displacement field between two time instants. It is based on tracking spatial variation of brightness between two images, one of which is usually recorded before applying any load (reference image) and one after deformation (deformed image). The displacement field is then determined by considering a segment or

Table 1
Concrete mix design details.

Coarse aggregate (5–12.5 mm)	936 kg/m^3
Sand (0–5 mm)	818 kg/m^3
Cement (Portland 52.5)	312 kg/m^3
Water	190 kg/m^3
Super plasticizer	0.8 kg/m^3

Table 2
Specimens geometry.

Beam		b (mm)	h (mm)	L (mm)	l (mm)	ρ (%)	Cover (mm)
Small	D1	100	100	400	300	1.99	10
Medium	D2	100	200	800	600	1.84	20
Large	D3	100	400	1600	1200	1.83	40

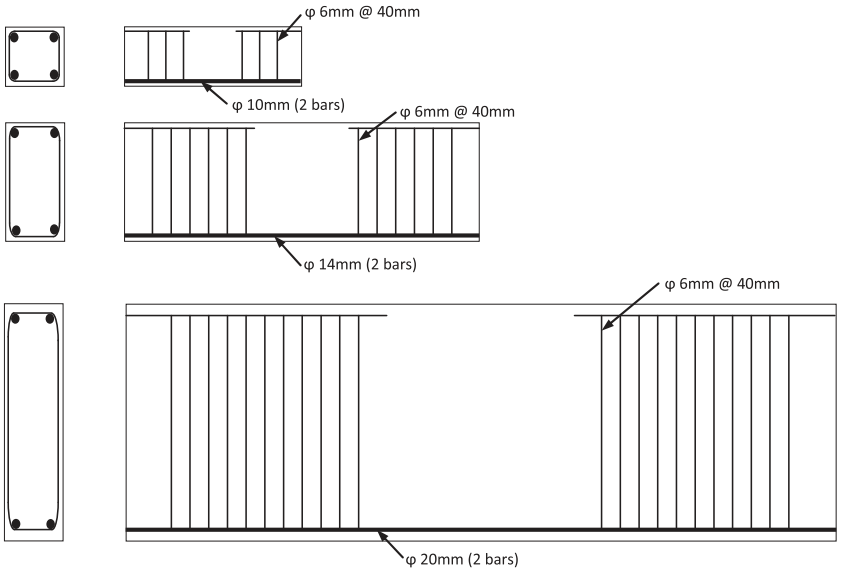

Fig. 1. Geometry and reinforcement details of D1, D2 and D3 beams.

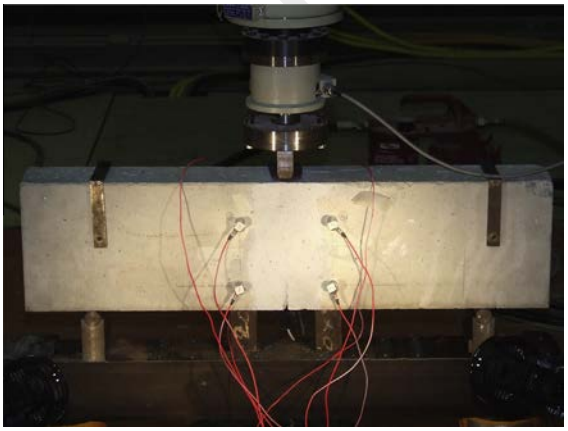

Fig. 2. Test setup.

sub image (29 × 29 pixels) in the reference image (1392 × 1040 pixels) and then locating this sub image in the deformed image, where the maximum likelihood is achieved. The technique has been established in mechanics of solids and concrete materials for displacement field measurement [12,26,13] and for measurement of crack openings [1]. Different approaches also make use of extended finite element principles to account for strong discontinuities [35]. For cracked solids, stress intensity factors were also determined from DIC measurements [38]. In our experiments, two cameras were placed in such a way to film an area of 150 × 100 mm by each camera on either side of the mid span. The mid span portion was filmed by both cameras. The mid span section was taken as the reference to relate the measurement values of the two cameras as shown in Fig. 4.

Fig. 3. Strain gauges attached to the steel bars.

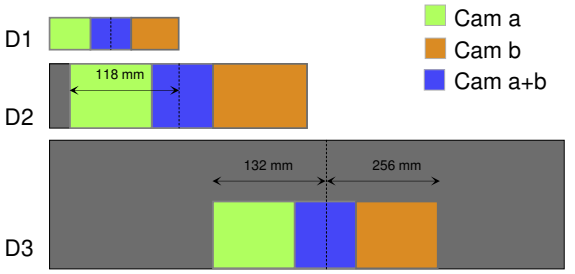

Fig. 4. Camera zones for DIC.

2.5. Acoustic Emission (AE) setup

In concrete, AE phenomenon is due to the creation of transient elastic waves resulting from internal micro displacements of the material. AEs are observed during the evolution of damage in concrete structures as well as crack detection. Several authors have studied the progress of acoustic activity depending on mechanical behaviour of the material [31,19,44,41,2]. In this study, the hypothesis made is following: A certain fraction of energy dissipated during fracture should be detected by AE system. The effects of material attenuation and reflections that alter the acoustic signals depend on the aggregate particle size and distribution. It is thus assumed that effects are constant for same type of concrete while changing the size of spec imen. The assessment of damage in reinforced concrete has been effectively performed by AE technique. A recent work has tried to locate the source origin based on the treatment of the acoustic signature [42]; but it was possible only by considering different exposure conditions. Ohtsu [29] investigated the relationship between failure modes and AE signal parameters. AE count rates in a beam exhibiting bending mode failure increase with increase in loading. However, in shear mode, AE count rates are observed at a constant rate until the final failure. Wu et al. [49] studied the mechanisms of cracking in mortar, con crete and reinforced concrete. They developed multiple filters on AE signal amplitude and arrival time to separate failure modes in these materials. Rao et al. [34] made use of amplitude to classify the microcracking initiation and extension and macrocracking initiation and extension. Ohtsu et al. [30] and Shiotani et al. [46] found that rise time is also an important AE parameter and is longer for shear cracks and shorter for tensile cracks.

The device used for the acquisition and signal processing of AE consists of a data acquisition system MISTRAS 8 channels. 3D AE analysis was performed for which 6 8 piezoelectric sensors (depending on the size of the sample tested) were employed with a frequency of 50 200 kHz and a resonance frequency of 150 kHz. The sensors were placed on the beam around the area of crack propagation. The sensors thus form a rectangular grid location (120×120 mm^2) on each side (Fig. 5) in all the beams. Thus, the distance in between the sensors was kept constant in all beams; however, in each beam the distance at the top and bottom part of the beam was adjusted to position the sensors so as to capture maximum acoustic data. The signals as detected by sensors were amplified by an amplifier with a gain of 40 dB. A detection limit of 35 dB was chosen to filter background noise [37]. The hit definition time used during the tests was set at 200 µs. The hit lockout time was equal to 500 µs which specifies time which must pass after a hit has been detected before a new hit can be detected and should be selected carefully to avoid reflections and late arriving component of the AE as hits. The acquisition system was calibrated before each test using a pencil lead break procedure HSU NIELSEN [37]. The acoustic wave propagation velocity measured in our study was 3800 m/sec. The Signal descriptors such as rise time, counts, energy, duration, amplitude, average frequency and counts to peak were calculated by AEwin® system. Each waveform was digitised and stored. The descriptors were further analysed and evaluated with Noesis® software.

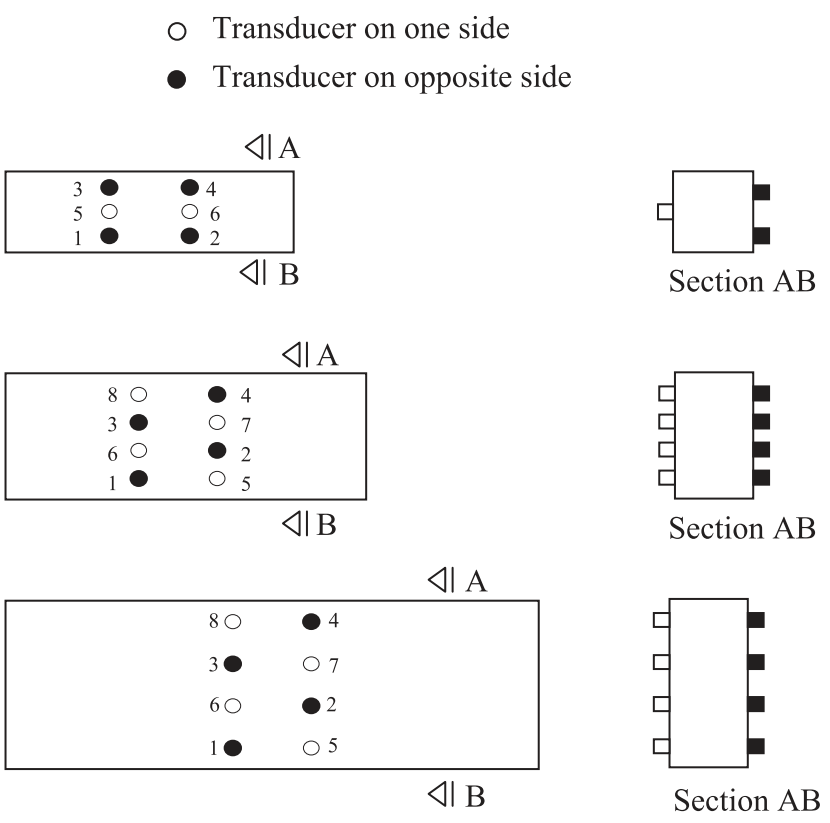

Fig. 5. Position piezoelectric sensors on the faces of the specimen.

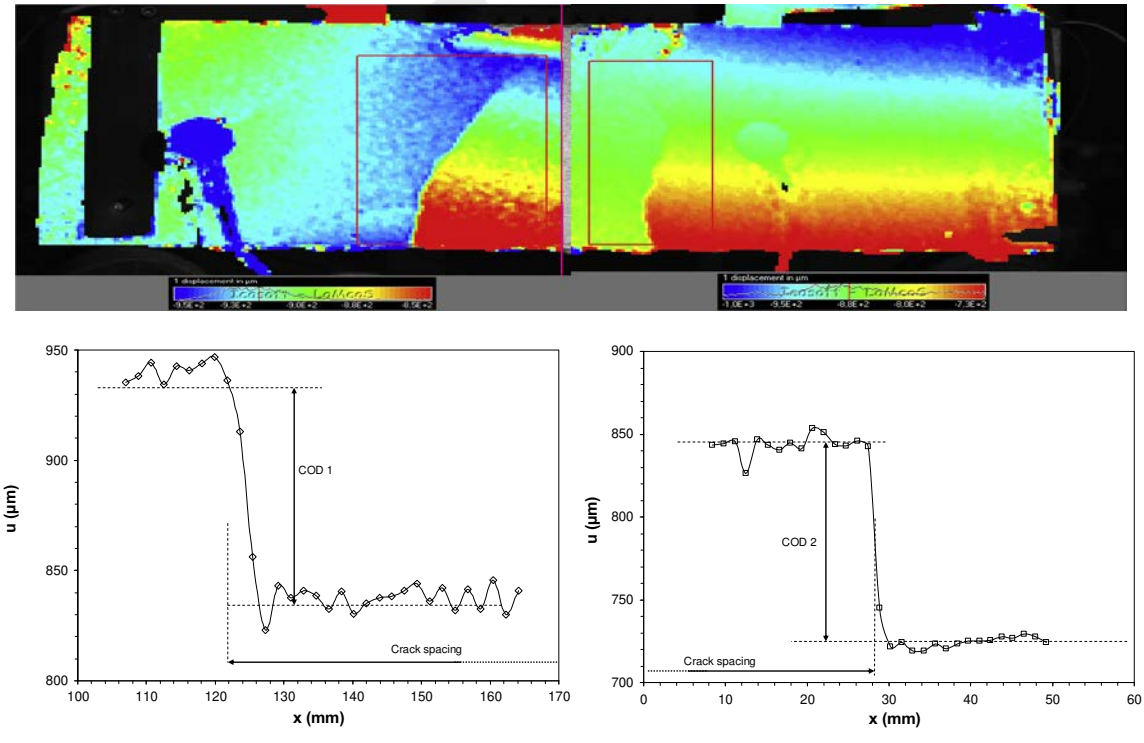

Fig. 6. Measurement of crack opening displacement (COD) and crack spacing in small (D1) beam.

3. Experimental results and discussion

3.1. Discrete crack features from DIC analysis

In the experiments, two techniques have been applied to register crack growth in the course of loadings. DIC technique was able to reproduce displacement field on the surface of specimens and discrete crack features: crack openings and crack spacing were extracted. The measurement of crack opening displacement (COD) and crack spacing in small concrete beam (D1) is presented in Fig. 6. COD was measured as displacement jump on the surface of beam [1]. Multiple cracks were found (3 5 cracks), but only maximum COD was considered for further analysis. The tensile strain in the bottom steel measured at mid span for all beams is presented in Fig. 7.

The crack openings and crack spacing obtained from the DIC analysis were compared with Eurocode [17]. The approach used in Eurocode (EC2 EN 1992) to explain the basic cracking behaviour of reinforced concrete is to consider cracking of a concrete prism reinforced with a central bar which is subjected to pure tension. Bending does influence the phenomena but this is dealt with in the Eurocode by an empirical adjustment of the coefficients. According to Eurocode (EC2 EN 1992), the design crack width can be determined using following expression.

$$w_k \quad s_{r,max}(\varepsilon_{sm} \quad \varepsilon_{cm}) \tag{1}$$

where w_k represents the design crack width, $s_{r,max}$ is the maximum crack spacing, ε_{sm} is the mean strain in the reinforcement and ε_{cm} is the mean strain in concrete between cracks.

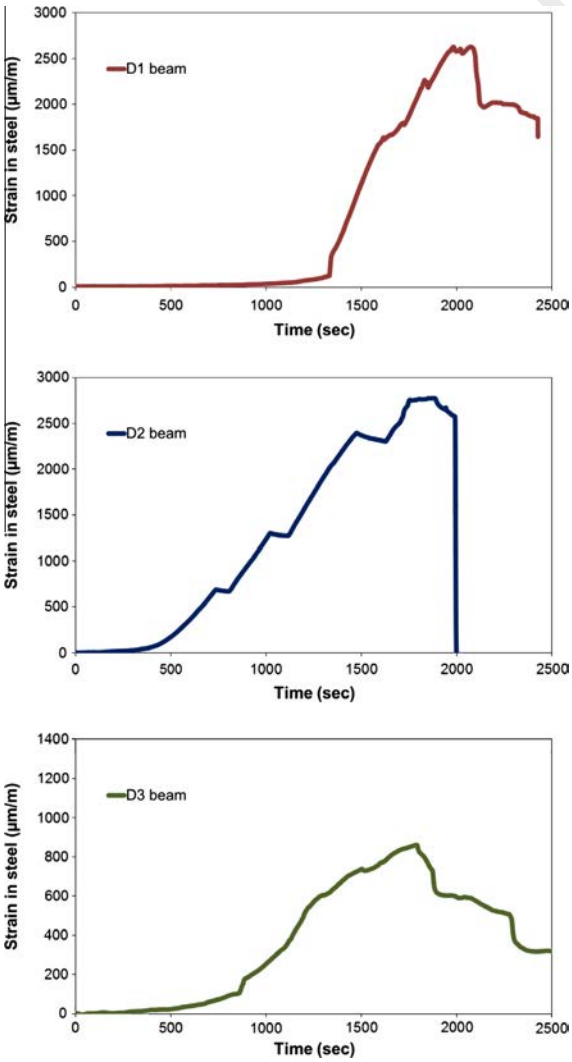

Fig. 7. Strain in steel at mid span in all beams.

In expression (1) (ε_{sm} ε_{cm}) may be calculated as:

$$\varepsilon_{sm} \quad \varepsilon_{cm} \quad \frac{\sigma_s \quad k_t \frac{f_{ct,eff}}{\rho_{p,eff}}(1+\alpha_e\rho_{p,eff})}{E_s} \geqslant 0.6\frac{\sigma_s}{E_s} \tag{2}$$

where σ_s represents stress in the tension reinforcement assuming cracked section, $\rho_{p,eff} = A_s/A_{c,eff}$, the ratio of area of tension reinforcement (A_s) to the effective tension area of concrete around the steel ($A_{c,eff}$). However, $A_{c,eff}$ depends implicitly upon the concrete cover provided on tension face. See details in EC2 EN 1992. When reinforcement is fixed at reasonably closed spacing (spacing $\leqslant 5(c + \phi/2)$), according to Eurocode (EC2 EN 1992) the maximum final crack spacing can be calculated as:

$$s_{r,max} \quad 3.4c + 0.425k_1k_2\frac{\phi}{\rho_{p,eff}} \tag{3}$$

where ϕ represents the bar diameter, c the concrete cover and k_1, k_2 the coefficients depending upon steel concrete bond properties and loading type respectively.

In Eq. (3) the concrete cover c is explicitly introduced into the expression of crack width as suggested by [7,8]. He studied the influence of concrete cover over the transfer length. The transfer length increases monotonically with the increase of con crete cover. This effect is introduced in the calculation of crack spacing. Stress in the concrete around the reinforcement is directly dependant on the stress transfer length between concrete and steel. Since cracking occurs in concrete at the points where stress exceeds the tensile strength of concrete, therefore, crack spacing is a function of concrete cover. In this study, concrete cover to height of the beam ratio is kept constant to take into account the effect of overall structure size on the crack opening and crack spacing.

It has been suggested that when analysing the test data of crack width and crack spacing in reinforced concrete tensile members, following considerations should be made (Commentary to EC2 EN 1992 [21]):

The low bound rebars, concrete qualities less than 20 N/mm^2 and steel qualities less than 400 N/mm^2 should not be used. The stress range should be serviceability range. For this purpose, results in the stress range in steel from 150 to 350 N/mm^2 should be considered for tests involving direct actions.
To determine the crack spacing the number of cracks present at the last phase of the test is always considered since it is the closest to the stabilized cracking, as given by (3).

The crack width measured using DIC technique is plotted against the crack width obtained using Eurocode crack width formula (1) as a function of steel strain ε_{sm}. The crack width is measured at the mouth of the crack i.e. at the lowest fibre of the beam where the crack width is maximum. The results are shown in Fig. 8 for comparison. It can be seen that Eurocode formula underestimates the crack width for all the three sizes. The difference between measured and calculated values exceed when the strain is higher.

A more detailed observation of the effect of structural size on Eurocode calculated crack opening is made in the Fig. 9. It is clear that the calculated crack width is more or less comparable for small size beam but the error exceeds when size increases. The crack width obtained from Eurocode formula does not take into account the effect of structural size. However, the values obtained are different for three sizes of beams. But, this should not be considered as the effect of struc tural size as the Eurocode formula depends only on the concrete cover and diameter of the bars, however, the true effect is the effect of the dimensions of the structure on the overall fracture mechanism. As the structure becomes sufficiently large the size of the heterogeneity becomes negligible compared to the size of the structure and material follows a brittle failure. However, when the size of the structure becomes sufficiently small the size of heterogeneity becomes comparable to the size of the structure and the material follows a ductile failure. The discrepancy in design values and experimental measurements is also due to the inherent assumption in Eq. (1) that the reinforcing steel is uniformly strained over the crack spacing.

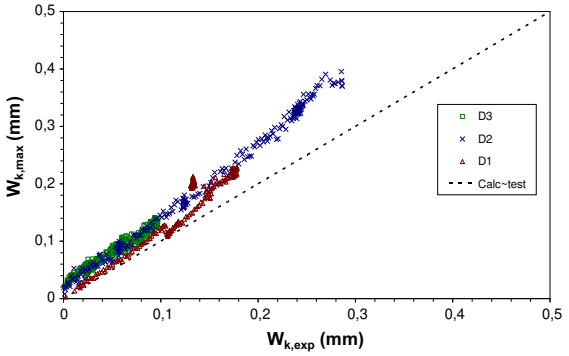

Fig. 8. Comparison of experimental crack opening ($W_{k,exp}$) and calculated maximum crack opening ($W_{k,max}$) during crack formation stage (ε_{sm} < yield limit).

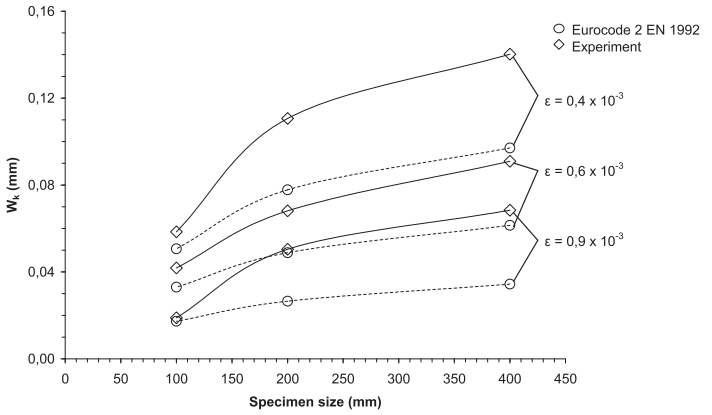

Fig. 9. Size effect on experimental and calculated maximum crack opening.

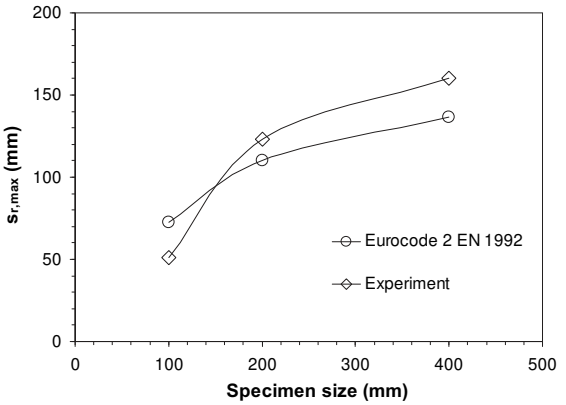

Fig. 10. Maximum spacing of cracks, comparison of measured values with the calculated values.

Experiments have shown that there are localised strain zone around the crack [47], thus the strain gradient in between the adjacent crack is neglected in the design equations. Therefore, Eq. (1) would underestimate the crack width under high strains.

The maximum spacing between cracks is also measured when steel stress was equal to 300 MPa. This spacing is com pared as shown in Fig. 10 with the spacing obtained from the Eurocode formula (3). It is seen that Eurocode underestimates the crack spacing for the medium (D2) and large (D3) sized beam. The reason may be that the concrete becomes more brittle when the size of the beam increases. Thus the crack propagation is much faster [1] and energy release rate is higher in large structures [25]. However for small structures, crack propagation is much slower and strain energy is mainly released due to microcracking in the fracture process zone. Since the presence of reinforcement hinders the development of fracture process zone, more cracks are being formed to release the strain energy stored in the material.

Other experiments also indicate that crack spacing increases with increasing load and stabilizes after reinforcement attains a certain critical stress [10,18]. As the loading further increases, the tensile cracks begin to widen and microcracking occurs at steel concrete interface. It has already been discussed that when size of the beam increases, failure mode changes from tensile to shear. Since the above analytic expressions (1 3) are developed for tensile mode failure considering a con crete prism reinforced with a central bar under tensile stress, different failure modes and the effect of structural size is intrin sically not considered and it would result into inaccurate estimation of crack spacing and crack opening.

3.2. Microcracking and AE analysis

In this section, the results of acoustic emissions are presented and discussed for beams D1, D2 and D3, respectively. AE parameters are accessed to have an in depth look into failure process in different sizes of beams. The results are presented in two steps. Initially, AE waveform parameters (hits and absolute energy) for each beam size are discussed (Figs. 11 13). Hits indicate the number of time each AE wave exceeded the threshold limit. Hits can be directly related to microcracking and sudden increase in hits count is related to macrocracking. Absolute energy is another important parameter. AE waves of high

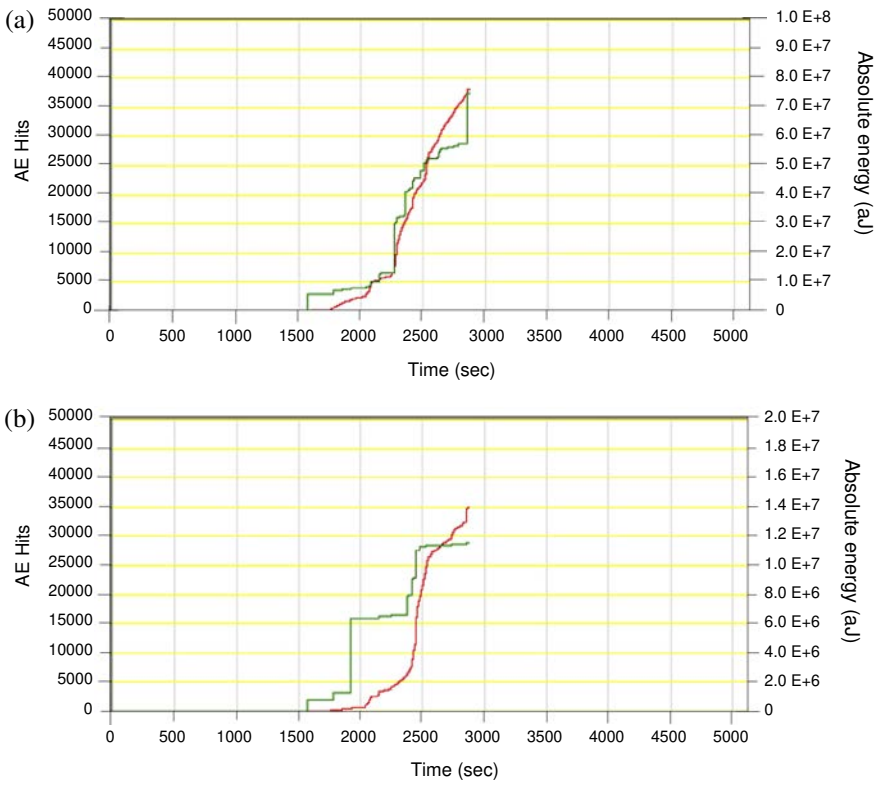

Fig. 11. AE waveform parameters for D1 beam (a) piezoelectric sensor #4 (b) piezoelectric sensor #1. Red line shows hit detected by the sensor; green line shows absolute acoustic energy of AE waveform. (For interpretation of the references to colour in this figure legend, the reader is referred to the web version of this article.)

absolute energy are generally accessed to indicate the formation of large fracture surfaces. We have presented here the results recorded by sensors 1 and 4 (bottom and top sensors). Other measurements obtained by the sensors show the similar effect.

In smaller specimen (D1) the bottom sensor indicates two jumps in AE energy. The first jump corresponds to low number of AE hits, which is related to microcracking in the bottom (tensile face) part of beam. However; the second jump corre sponds to large number of AE hits which should be related to the macrocracking and propagation of cracks. It should be noted that between the two jumps, AE energy does not increase while there is a slight increase in AE hits. This phase may be related to microcracks which are usually less energetic. Along with the second jump in AE energy of bottom sensor, the top AE sensor have shown a smooth increase in AE energy and AE hits, which is due the macrocrack propagation from bottom to the top part of the beam. This can be correlated with the physical examination of specimen which showed failure due to diagonal cracks development from bottom to the top part of the beam.

In the medium specimen (D2), the development of AE energy and hits is very small until the first jump of AE energy occurring simultaneously in the top and bottom sensors. Thus, unlike D1 beam, the fracture initiates by macrocracking (diag onal macrocracks were observed physically). Further from this point, the bottom sensor recorded increase in AE energy in smaller jumps with concurrent smooth increase in AE hits, which indicates development of tensile macrocracking.

In larger specimen (D3), the top AE sensor recorded an increase in AE hits with low AE energy (microcracking). The major AE energy release is in the form of a sudden jump, which indicates macrocracking (compression failure). The bottom sensor shows a smooth increase in AE energy and AE hits which indicates microcracks in the bottom part of the beam.

It appears that as the size of beam increases, the fracture process changes from tensile microcracking macrocracking to shear compression macrocracking. The evolution of the energy released due to microcracks shows the same pattern. The energy released is smaller at the peak load when increasing the size of the beam. As noted above, developments and bursts of energy are in steps (more or less pronounced). This describes the rate of increase of acoustic phenomena. High rate of development of AE is indicative of a softening phase in the mechanical behaviour. This is due to the cohesion of the phases of the material that hinders the development of cracks.

In the preceding section it was found that different AE parameters and damage mechanisms can be interrelated. Another approach to improve the identification of damage mechanisms is by using multi parametric analysis. In this regard, different approaches were developed e.g. pattern recognition [22], *K means* algorithm [27] and principal component analysis [23].

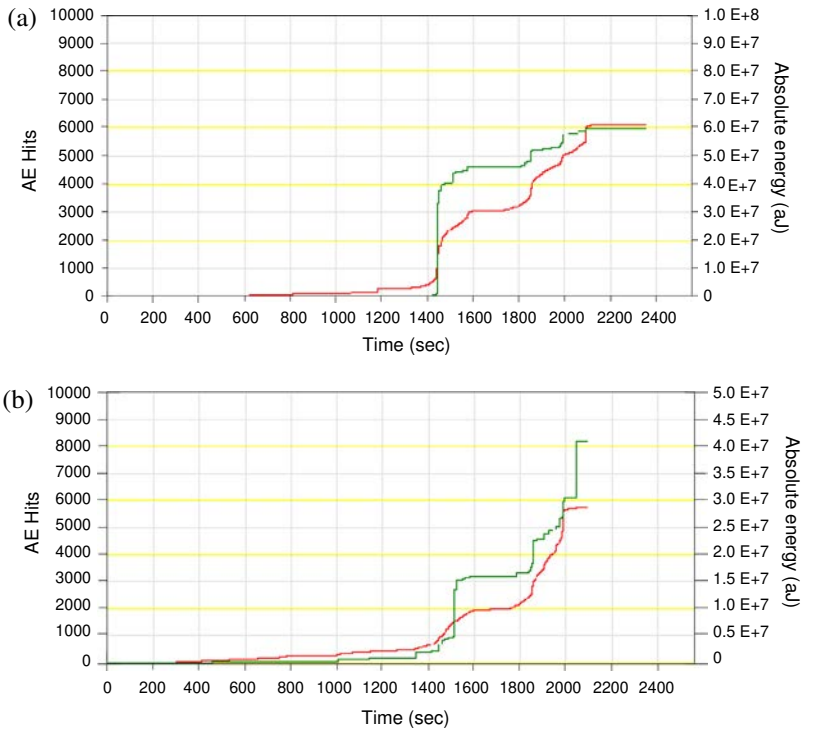

Fig. 12. AE waveform parameters for D2 beam (a) piezoelectric sensor #4 (b) piezoelectric sensor #1. Red line shows hit detected by the sensor; green line shows absolute acoustic energy of AE waveform. (For interpretation of the references to colour in this figure legend, the reader is referred to the web version of this article.)

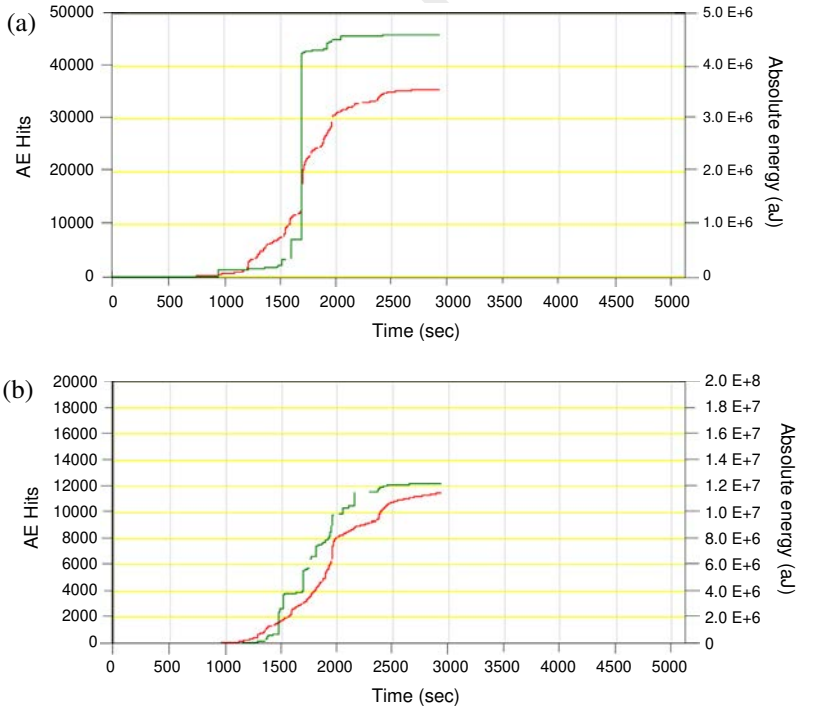

Fig. 13. AE waveform parameters for D3 beam (a) piezoelectric sensor #4 (b) piezoelectric sensor #1. Red line shows hit detected by the sensor; green line shows absolute acoustic energy of AE waveform. (For interpretation of the references to colour in this figure legend, the reader is referred to the web version of this article.)

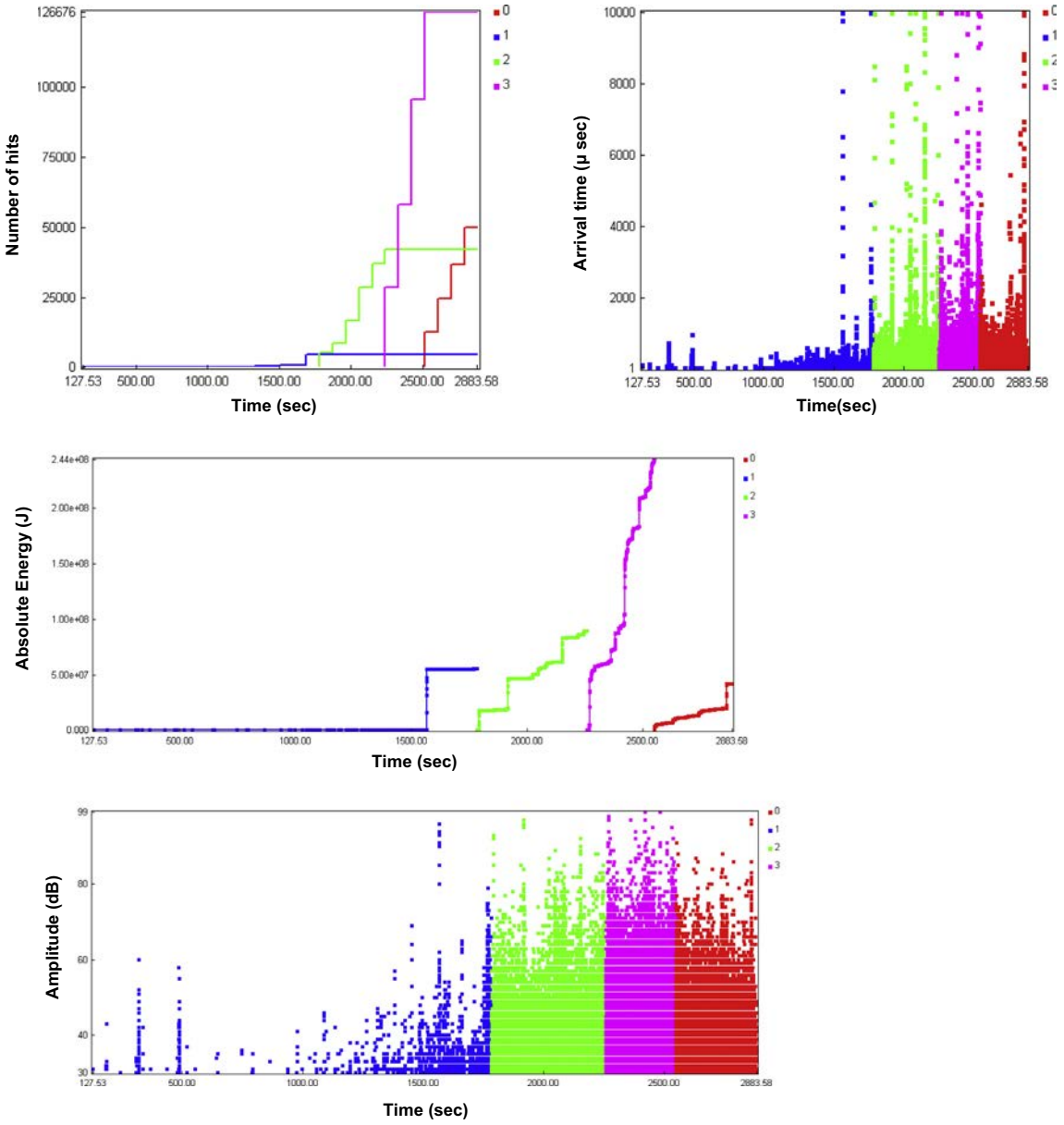

Fig. 14. Evolution of acoustic parameters versus time for D1 beam.

Another study based on intensity analysis, relaxation ratio and *b* value analysis is presented in [15]. The *K means* method is a solution of the clustering problem which is defined as the problem of finding homogeneous groups (or classes) of data points in a given data set. In this study, a manual grouping method (similar to *K means* method) was employed based on different stages of evolution of the absolute energy of AE as a function of time (Figs. 14 16). It allowed better visualisation of the tem poral characteristics of signals and displaying for each beam, groups of AE activity corresponding to each stage of material failure. In the following, four measures over time are presented for each beam: arrival time of acoustic waves associated with an event, number of hits, absolute energy and amplitude.

In the smaller beam (D1) (Fig. 14), the first class between times $t = 0$ sec and $t = 1750$ s, represents the AE activity of low energy. The number of AE hits is low and arrival time is very less. This AE activity is associated with the elastic phase of rein forced concrete where at the same time the deformation of the reinforcement increases linearly (<78% of max. elongation). In the second class (∼1750 2250 sec) the AE energy increases stepwise and steadily through the increase in the number of hits as well as their duration and amplitude, which indicates microcracking phase. The third class from 2250 to 2550 sec, the AE energy increases very rapidly and the number of AE hits (126 676) increases in a very short time. The amplitudes and dura tions remain substantially constant. This strong increase of energy takes place when the strain in steel drops as measured by

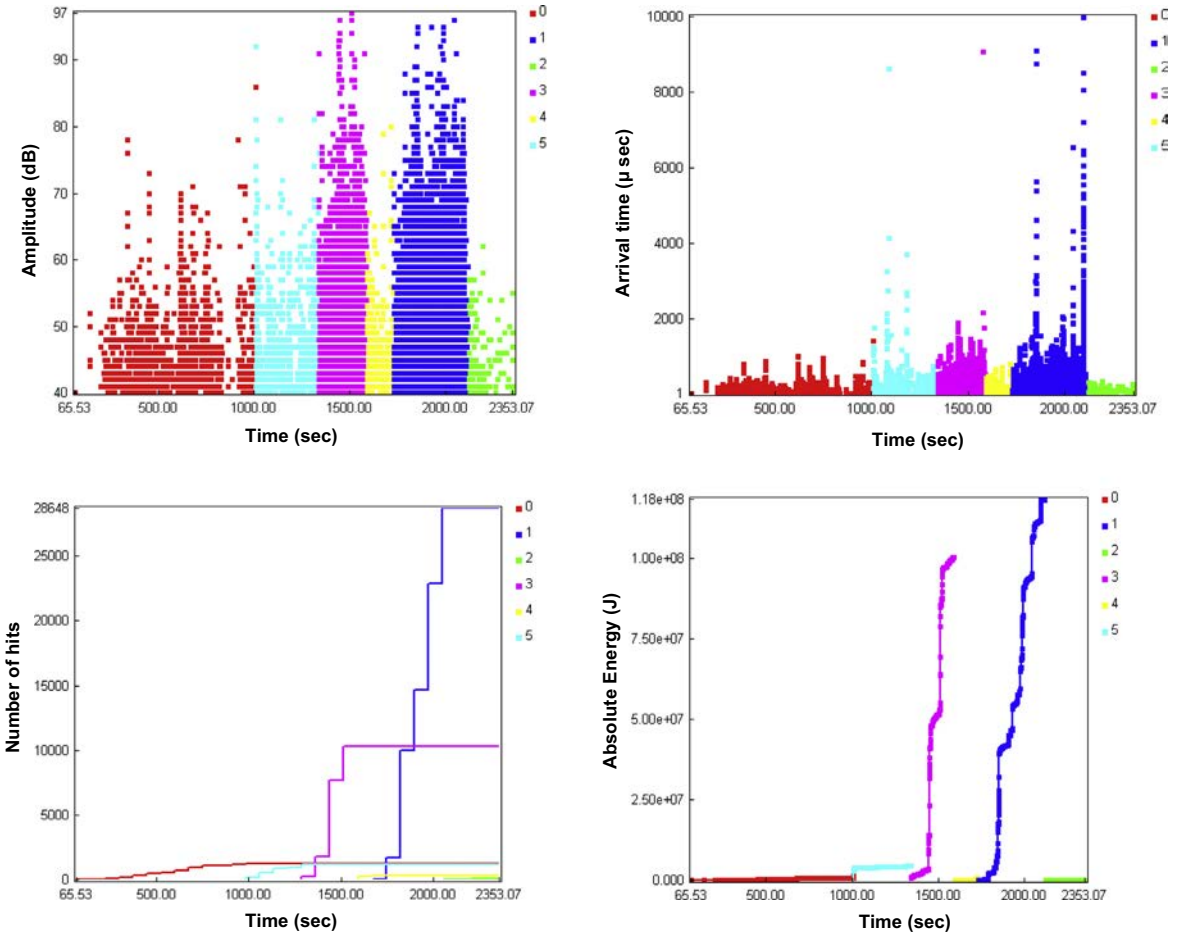

Fig. 15. Evolution of acoustic parameters versus time for D2 beam.

the embedded strain gauges. The increase in AE energy indicates macrocrack propagation. This may also result into failure of the concrete in contact with the reinforcement. Finally, during the last period (2550 2883 sec), the acoustic energy increase is very small. A certain (small) increase in number of hits is detected while the amplitudes of acoustic signals decrease with respect to the previous period. This phase may indicate further crack openings.

In D2 beam (Fig. 15), during the first two classes (0 1400 sec) the amplitudes measured are average and of very short durations, that results into an AE energy that does not increase. The phase may indicate the initial elastic response of the beam. AE energy then increase significantly in the next classes (3rd and 5th) and two peaks can be identified. The first peak seems to correspond to the reduction of strain in steel reinforcement. Between these peaks are observed period of rest during which the amplitudes and arrival time are extremely low. This stage may correspond to the resumption of stresses by the reinforcement. It can be said that in these phase two (or more) macrocracks may have been formed.

In larger (D3) beam (Fig. 16), the first class (0 to $\sim$ 800 sec), there is almost no AE energy recorded, which indicates the elastic phase. The next two classes ($\sim$800 to 2200 sec) show a significant increase in AE activity. Thus macrocrack propaga tion occurs in the specimen. No class of microcracking (unlike D1 and D2 beams) is observed in D3 beam before the macro cracking. The evolution of all parameters may indicate the deformation of the steel reinforcement and rupture of bond between steel and concrete. On reaching the peak load (2250 sec), also corresponding to the maximum strain measured, the AE energy increases sharply and also the number of hits detected and the duration of the acoustic events increases.

The above results show that larger the beam, higher is the number of steps in which the failure occurs (calculated number of classes). Also, these steps are longer in time for large beams. The results presented confirm the fact that large beams behave more brittle i.e. little or no microcracking before the macrocrack propagation and high energy release at peak load. However, smaller beams have more ductile behaviour with distinct microcracking phase before the macrocrack propagation. It should also be noticed that the fracture zone in reinforced concrete is more complex and wider. A larger specimen size may seem more appropriate for fracture zone analysis and the effect of structural size.

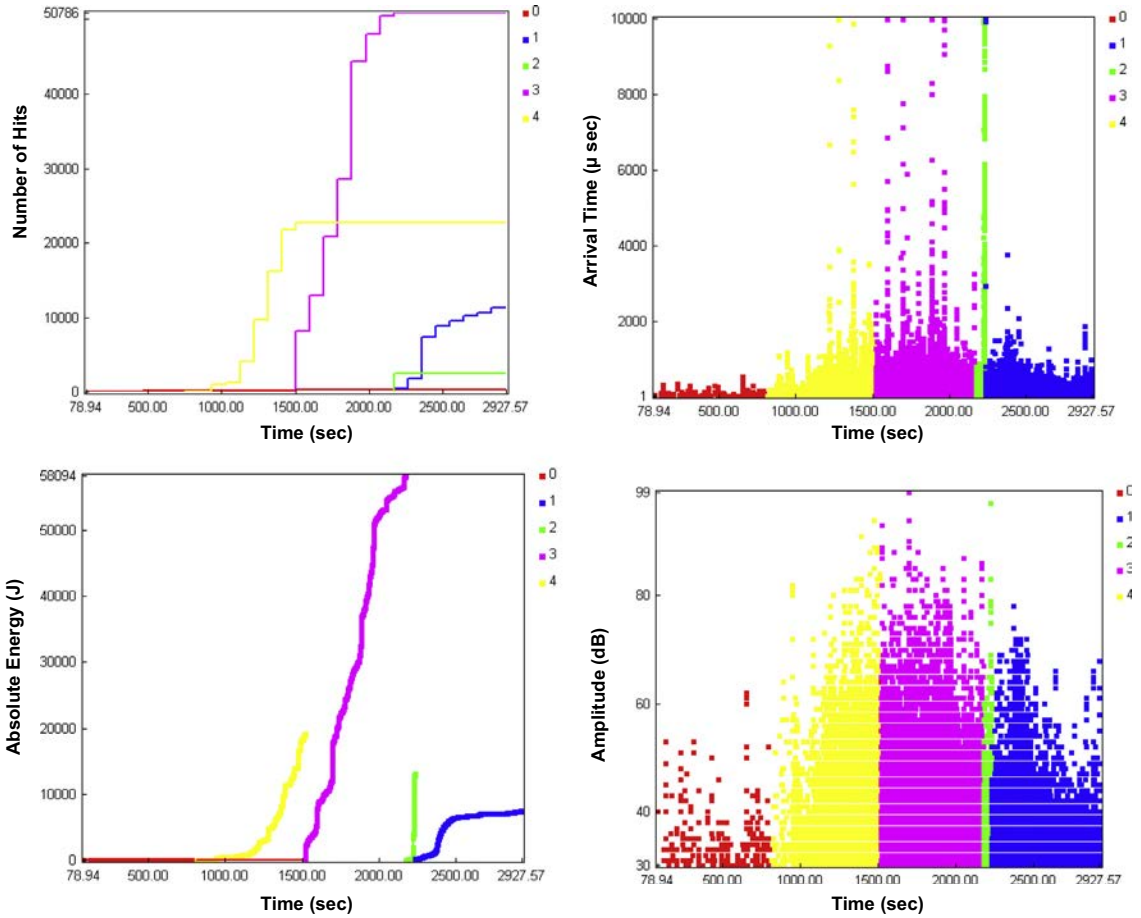

Fig. 16. Evolution of acoustic parameters versus time for the beam D3.

4. Conclusions

In this paper, bending tests were performed on reinforced concrete beams. DIC and AE techniques were applied to identify the mechanisms of cracking of concrete and to evaluate the influence of the structural size.

In the first part of the study, Eurocode expressions for crack openings and cracks spacing are evaluated and compared with experimental measurements under service loading. The results show that the measured values more or less agree with the calculated values at low strains and for the smallest beam size. However, as the strain increases, the Eurocode expres sions underestimate the crack openings and spacing. The discrepancy between Eurocode estimation and experimental mea surements of crack openings and crack spacing increases as the size of the beam increases. It seems that difference in experimental results and design expressions is due to the shift in failure modes observed when the size of the specimen increases, which is not taken in account in expressions.

In the second part of the study, microcracking is studied through AE parametric analysis. AE hits and AE energy are anal ysed in the top and bottom sensors. It appears that larger the beam size, the number of hits and AE energy released are low during the initial loading stages. The AE energy release is more abrupt in larger beam (D3) at peak load, while in the smaller beams it is quasi continuous.

A manual grouping method (similar to *K means* method) is used to identify different classes of AE energy released. For these classes, AE parameters are analysed to identify microcracking and macrocracking phases when the size increases from small to large beams.

A crack classifying procedure is adopted to distinguish between AE waves resulting from tensile cracking and shear crack ing. In the larger beam, tensile microcracking is observed initially; however, other beams show tensile and shear microcrack ing in the initial and intermediate level of loadings. In the final stages shear cracking is more pronounced.

The conclusions are based on the results obtained on 1:3 scale. As the fracture process is more complex in reinforced con crete as compared to plain concrete, more conclusive results may be obtained on a wider scale.

References

[1] Alam SY, Loukili A, Grondin F. Monitoring crack openings in concrete beams with different sizes using digital image correlation technique. Eur J Environ Civil Engng 2012;16(7):818–36.
[2] Alam SY, Saliba J, Loukili A. Fracture examination in concrete through combined digital image correlation and acoustic emission techniques. Constr Build Mater 2014;69:232–42.
[3] Bazant ZP, Oh BH. Crack band theory for fracture of concrete. Mater Struct 1983;16:155–77.
[4] Bazant ZP. Size effect in blunt fracture: concrete, rock, metal. J Engng Mech (ASCE) 1984;110(4):518–35.
[5] Bazant ZP, Kim J-K. Size effect in shear failure of longitudinally reinforced beam. ACI J Proc 1984;81(5):456–68.
[6] Bazant ZP, Kazemi MT. Size effect on diagonal shear failure of beams without stirrups. ACI Struct J 1991;88(3):268–76.
[7] Beeby AW. Calculation of crack width, PrEN 1992–1 (final draft), chapter 7.3.4. Technical report, 2001a.
[8] Beeby AW. Crack control provisions in the new Eurocode for the design of concrete structures. ACI Spec Publ 2001;204:57–84.
[9] Brincker R, Henriksen MS, Christensen FA, Heshe G. Size effects on the bending behaviour of reinforced concrete beams. Eur Struct Integrity Soc 1999;24:127–37.
[10] Broms BB. Crack width and crack spacing in reinforced concrete members. ACI J Proc 1965;62(10):1237–55.
[11] Chana PS. Some aspects of modelling the behavior of reinforced concrete under shear loading. Technical report No.453, Cement and Concrete Association, Wexham Springs; 1981.
[12] Choi S, Shah SP. Measurement of deformations on concrete subjected to compression using image correlation. Exp Mech 1997;37:307–13.
[13] Corr D, Accardi M, Graham-Brady L, Shah SP. Digital image correlation analysis of interfacial debonding properties and fracture behaviour in concrete. Engng Fract Mech 2007;74(1–2):109–21.
[14] Duan K, Hu X, Wittmann FH. Size effect on specific fracture energy of concrete. Engng Fract Mech 2007;74:87–96.
[15] ElBatanouny MK, Ziehl PH, Larosche A, Mangual J, Matta F, Nanni A. Acoustic emission monitoring for assessment of prestressed concrete beams. Constr Build Mater 2014;58:46–53.
[16] El-Hachem R, Rozière E, Grondin F, Loukili A. New procedure to investigate external sulphate attack on cementitious materials. Cement Concr Compos 2012;34(3):357–64.
[17] European Committee for Standardization (CEN), Brussels. Eurocode 2: Design of concrete structures – Part 1–1: General rules and rules for buildings, December 2004.
[18] Frosch RJ. Another look at cracking and crack control in reinforced concrete. ACI Struct J 1999;96(3):437–42.
[19] Granger S, Loukili A, Pijaudier-Cabot G, Chanvillard G. Experimental characterization of the self-healing of cracks in an ultra high performance cementitious material: mechanical tests and acoustic emission analysis. Cem Concr Res 2007;37(4):519–27.
[20] Ichinose T, Kanayama Y, Inoue Y, Bolander Jr JE. Size effect on bond strength of deformed bars. Constr Build Mater 2004;18(7):549–58.
[21] Jacobs JP. Commentary Eurocode 2. Technical report, European Concrete Platform ASBL, Brussels; June 2008.
[22] Johnson M. Waveform based clustering and classification of AE transients in composite laminates using principal component analysis. NDT E Int 2002;35:367–76.
[23] Jolliffe IT. Principal component analysis. Springer Verlag; 2002.
[24] Kani GNJ. How safe are our large concrete beams? ACI J Proc 1967;64(3):128–42.
[25] Kaplan MF. Crack propagation and the fracture concrete. ACI J 1961;58(11).
[26] Lawler JS, Keane DT, Shah SP. Measuring three-dimensional damage in concrete under compression. ACI Mater J 2001;98(6):465–75.
[27] Likas A, Vlassis N, Verbeek J. The global *k*-means clustering algorithm. Pattern Recogn 2003;36:451–61.
[28] Luccioni BM, López DE, Danesi RF. Bond-slip in reinforced concrete elements. ASCE J Struct Engng 2005;131(11):1690–8.
[29] Ohtsu M. Acoustic emission characteristics in concrete and diagnostic applications. J Acoust Emiss 1987;6(2):99–108.
[30] Ohtsu M, Uchida M, Okamoto T, Yuyama S. Damage assessment of reinforced concrete beams qualified by acoustic emission. ACI Struct J 2002;99(4):411–7.
[31] Otsuka K, Date H. Fracture process zone in concrete tension specimen. Engng Fract Mech 2000;65(2–3):111–31.
[32] Ouyang C, Shah SP. Fracture energy approach for predicting cracking of reinforced concrete tensile members. ACI Struct J 1994;91:69–78.
[33] Picandet V, Khelidj A, Bellegou H. Crack effects on gas and water permeability of concretes. Cem Concr Res 2009;39(6):537–47.
[34] Rao GMN, Murthy CRL, Raju NM. Characterization of micro and macro in rocks by acoustic emission. In: Vahaviolos, editor. Acoustic emission: standards and technology update. ASTM STP 1353. American Society for Testing and Materials; 1999.
[35] Réthoré J, Hild F, Roux S. Extended digital image correlation with crack shape optimization. Int J Numer Meth Engng 2008;72:248–72.
[36] RILEM Recommendation. Size-effect method for determining fracture energy and process zone size of concrete. Mater Struct 1990;23:461–5.
[37] RILEM TC212-ACD Recommendation. Acoustic emission and related NDE techniques for crack detection and damage evaluation in concrete. Mater Struct 2010;43:1177–81.
[38] Roux S, Réthoré J, Hild F. Digital image correlation and fracture: an advanced technique for estimating stress intensity factors of 2d and 3d cracks. J Phys D Appl Phys 2009;42(21):214004.
[39] Rozière E, Loukili A, El-Hachem R, Grondin F. Durability of concrete exposed to leaching and external sulphate attack. Cem Concr Res 2009;39(12):1188–98.
[40] Ruiz G, Elices M, Planas J. Size effect and bond-slip dependence of lightly reinforced concrete beams. Eur Struct Integrity Soc 1999;24:67–97.
[41] Saliba J, Loukili A, Grondin F. Study of creep-damage coupling in concrete by acoustic emission technique. Mater Struct 2012;45(9):1389–401.
[42] Saliba J, Loukili A, Grondin F, Regoin JP. Identification of damage mechanisms in concrete under high level creep by the acoustic emission technique. Mater Struct 2014;14(6):1041–53.
[43] Shah SP, Swartz SE, Ouyang C. Fracture mechanics of concrete: applications of fracture mechanics to concrete, rock and other quasi-brittle materials. New York: Wiley; 1995.
[44] Shah SP, Choi S. Nondestructive techniques for studying fracture processes in concrete. Int J Fract 1999;98:351–9.
[45] Shioya T, Akiyama H. Application to design of size effect in reinforced concrete structures. In: Mihashi H, Okamura H, Bazant ZP ZP, editors. Size effect in concrete structures. London: Spon; 1994. p. 409–16.
[46] Shiotani T, Ohtsu M, Ikeda K. Detection and evaluation of AE waves due to rock deformation. Constr Build Mater 2001;15:235–46.
[47] Syroka-Korol E, Tejchman J. Experimental investigations of size effect in reinforced concrete beams failing by shear. Engng Struct 2014;58:63–78.
[48] Taylor HP. Shear strength of large beams. ASCE J Struct Div 1972;98(11):2473–89.
[49] Wu K, Chen B, Yao W. Study on the AE characteristics of fracture process of mortar, concrete and steel-fiber-reinforced concrete beams. Cem Concr Res 2000;30:1495–500.
[50] Yi ST, Kim MS, Kim JK, Kim JHJ. Effect of specimen size on flexural compressive strength of reinforced concrete members. Cement Concr Compos 2007;29(3):230–40.